Fire-induced flows for complex fire scenarios in a mechanically ventilated two-storey structure

Hugues Prétrel, Samuel Vaux

Fire-induced flows for complex fire scenarios in a mechanically ventilated two-storey structure

Hugues Prétrel and Samuel Vaux

Institut de Radioprotection et de Sûreté Nucléaire (IRSN), PSN-RES/SA2I, Cadarache, St Paul-Lez-Durance, 13115 France

---

Highlights:

- Fire-induced flow for complex fire scenarios in a mechanically ventilated assembly of enclosures
- Comparative analysis of bi-directional flows at doorways and vent
- Performance of CFD numerical tools compared with experimental data

Abstract:

This work deals with smoke propagation through a multi-compartment assembly in case of a fire event in a nuclear installation. The scientific issues are the understanding of flows involving two modes of propagation (vent and doorway), together with the role of mechanical ventilation and oxygen backflows to the fire. The study is based on the analysis of two scenarios reproduced experimentally at large scale and simulated numerically. The main outcomes concern the comparison of the flow at a doorway and at a vent, the consequence of the smoke propagation for thermal stratification and the combined effect of the fire heat release rate and mechanical ventilation. The results highlight the performance of CFD simulations in predicting these complex scenarios. Low-velocity flow zones are identified, enabling the structure of these flows and their amplitudes to be quantified. This information provides new insights to improve fire risk assessment in nuclear facilities.

Keywords:

smoke, propagation, ventilation, multi-compartment, doorway, vent

1 Introduction

Fire-induced flows represent an important issue in the assessment of fire risk in nuclear installations. In particular, the temperature field and soot concentration field are variables of interest that need to be accurately estimated to assess the risk of (1) malfunction of safety-relevant equipment, (2) release of radioactive aerosols or (3) radioactive soot deposition in the enclosures. Moreover, in the case of fire scenarios in closed, mechanically ventilated rooms, flows also have a feedback effect on the fire and the combustion zone, modulating the amount of oxygen that feeds the fire. Fire-induced flows are mainly controlled by buoyancy forces induced by the temperature differences inside the compartments. In the case of mechanically ventilated compartments, flows are also influenced by the pressure differences induced by the ventilation network. In nuclear installations, a typical fire scenario may involve several rooms connected by doorways or horizontal vents and mechanically ventilated to ensure their dynamic confinement. These issues call for ongoing evaluation of the predictive performance of these flows.

The state of the art in fire-induced flows in a room is substantial. Early studies focused on a single room naturally ventilated through an opening (doorway or vent) [1] [2]. The variables of interest were the thermal plume feeding the smoke layer, the vertical thermal stratification with a hot smoke layer at the top, the ceiling jet flow and the inflow and outflow at an opening. In the first step, correlative approaches were proposed to predict plume flow, smoke layer temperatures and flow rates at openings [3], [4] [5], [6]. Based on these approaches, a global model established on a two-zone description emerged in the fire science community and was implemented in zone codes [7] [8]. The global model was initially developed for the natural convection regime; the effects of mechanical ventilation were soon taken into account [9]. To understand the behaviour of a fire in a mechanically ventilated compartment, it was essential to study the combined effects of buoyancy and inertia on smoke propagation [10]. The influence of changing ventilation settings during the course of a fire was also studied [11]. Subsequently, the emergence of CFD simulation approaches in the 1990s allowed a more detailed spatial description of the flows [12]. These studies were extended to more complex scenarios involving several rooms of different shapes, which are configurations frequently encountered in nuclear installations. In the OECD/NEA PRISME project initiated in 2008, large-scale experiments were carried out, focusing in particular on the propagation of smoke through openings and the influence of mechanical ventilation. Using the results of this project, the performance of several simulation tools such as zone codes CFAST [13], MAGIC from EdF [14], and SYLVIA from IRSN [15] and CFD codes such as SATURNE from EdF [13], CALIF^{3}S-Isis from IRSN [16], [17], [18], [19], [20], FDS from NIST [21], [22] or OpenFoam [23] [24] were able to be evaluated.

The objective of the present study is to propose a new contribution to the work on fire-induced flows by addressing a complex scenario involving a set of mechanically ventilated rooms connected to each other by doorways and a horizontal vent. An innovative aspect of this study is to address flows in rooms which are not mechanically ventilated and in which the flows are driven solely by buoyancy. For example, this situation may be encountered when the ventilation of the rooms involved in the fire is stopped. These rooms can be referred to as dead zones from the ventilation point of view. The flow is low-turbulence and therefore difficult to predict numerically and very few contributions dealt with this no-ventilation regime. The challenge of dead zones is firstly to investigate the performance of computational fluid dynamics (CFD) simulation for low-velocity zones, and secondly to provide input data for assessing soot deposition within the enclosures.

The study is based on two fire scenarios representative of practical situations encountered in the nuclear installation and defined jointly by all partners of the OECD/NEA PRISME3 project. These scenarios were experimentally reproduced at large scale and numerically simulated with the CFD CALIF^{3}S-Isis IRSN software. In the first part of the article, the experiments and the numerical tool are described. The results then focus on the description of the fire source, the thermal stratification in the rooms, the flows at the openings and the velocity fields in non-ventilated rooms considered as dead zones.

2 Materials and methodology

2.1 Description of the fire scenarios

Two representative fire scenarios were considered in an assembly of three adjacent rooms and an upper room, as illustrated in Fig. 1. The fire room is the right-most room connected to the other rooms with a doorway and the vent. The objective of the first one named A1 was to study flows in rooms not mechanically ventilated (rooms L1 and L2) and flows in a fire room (L3) only naturally ventilated with a doorway and a vent. Only the upper room L4 was ventilated and was the only source of oxygen supply of the fire room. The fire size is designed small enough (0.4 m^2 pool fire) to avoid rapid extinction of the fire due to the lack of oxygen. This configuration reproduces the situation of a fire in an assembly of rooms (here the three adjacent rooms connected to each other). In this assembly, the ventilation is stopped because of the fire, but remains connected to another area (here represented by the upper room) for which the ventilation remains in operation. The benefit of this configuration is that it provides information about the downward fresh air flow at the vent that feeds the fire as well as the dead zones in the naturally ventilated

rooms. The objective of the second scenario A2 was also to study flows in rooms not mechanically ventilated (L1, L2 and L4) and in which smoke is only supplied naturally through two types of openings, a doorway, and a horizontal vent. The fire source was positioned in the only mechanically ventilated room. In this case, the pool dimension was designed large enough (1 m^2 pool fire) to ensure a long, sooty fire. In both scenarios, an additional objective was to investigate smoke flow in rooms only naturally ventilated, in which a dead zone situation with low velocity amplitude can be expected.

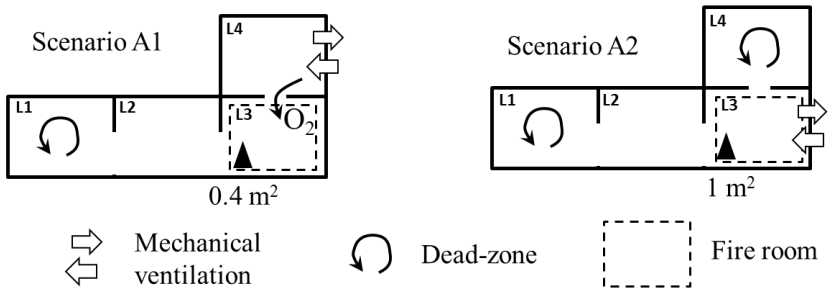

Fig. 1. Illustration of the two scenarios investigated

2.2 Experimental fire tests

The two scenarios were conducted experimentally in a set of closed, mechanically ventilated rooms belonging to IRSN's DIVA facility. The two scenarios comprised four rooms (named L1, L2, L3 and L4) connected by two doorways named L2L1 and L3L2 (height H_d=2.17 m and width 0.79 m) and a square vent (1.1 m wide) as illustrated in Fig. 2. The three rooms L1, L2 and L3 were identical, with a volume of approximately 111 m^3 (height H_1 = 3.84 m, length L_1 = 4.9 m, width w_1 = 5.9 m). Room L4 with a volume of 157 m^3 (Height $H_2 = H_1$, length L_2 = 4.86 m, width w_2 = 8.38 m) was located above one of the three rooms and connected to it by a horizontal vent. The walls were made of 300 mm or 350 mm thick concrete. To provide thermal protection, the ceiling consisted of concrete, an air gap and two insulating panels: Board Plus LTI insulated panels (10 mm) and "Monalite M1A" calcium silicate panels (13 mm, ρ = 720 kg/m^3, k = 0.19 W/K/m, Cp = 960 J/kg/K). Illustrations of the facility are shown in Fig. 3. The facility was equipped with an industrial ventilation network. Two ventilation layouts were set for the scenarios A1 and A2 and are shown in Fig. 1. For the scenario A1, only one adjacent room, upper room L4, was mechanically ventilated. The other rooms, including the fire room, were not ventilated. For scenario A2, only fire room L3 was mechanically ventilated; the other rooms were naturally ventilated through the openings. For both scenarios, the inlet and exhaust were positioned at the top of the rooms as shown in Fig. 2. The targeted air flow rate prior to ignition was 2,400 m^3/h for both tests, which corresponds to an air change rate per hour (ACH) of about 4.9 h^{-1} based on the total volume of the four rooms (about 490 m^3).

The fire source was a lubricating oil pool fire (Mobile DTE MEDIUM) to be representative of fuels encountered in nuclear installations and already used in previous studies [25], [19], [26]. The chemical formula of the fuel was $C_{31}H_{64}$, the boiling temperature 480°C, the molar mass 440 g/mol and the density at 20°C of 0.87 g/ml. The effective heat of combustion was considered to be 37.3 MJ/kg, deduced from open atmosphere fire tests [27]. This value is slightly lower than the value of 42.7 MJ/kg deduced from laboratory tests [26]. Two pool sizes were considered, 0.4 m^2 and 1 m^2 for scenarios A1 and A2 respectively. The fire source was in the north-west corner of room L3 (see Fig. 2), to avoid having the fire plume axis right below the vent. The pan was circular and made of carbon steel with a fixed depth of 150 mm. The fuel was ignited with a 60-kW propane gas burner.

The fuel mass loss was measured with a SARTORIUS IS300 IGG weighing device. The mass loss rate (MLR) was calculated as the time derivative of the mass loss signal. Smoke and air flows within the rooms were characterized by the temperature. Gas temperatures were measured with K-type thermocouples distributed over five vertical masts located in each room and equipped with nine probes positioned at 0.05 m,

0.55 m, 1.05 m, 1.55 m, 2.05 m, 2.55 m, 3.05 m, 3.55 m and 3.80 m from the ground as illustrated in Fig. 2. To measure the bidirectional flow through the doorway, vertical masts equipped with seven temperature and velocity probes were considered. Similar measurements (14 points) were distributed over the vent section. Pressure, temperature and volume flow rates were also measured in the supply and exhaust ventilation lines. The measurement acquisition frequency was 1 Hz.

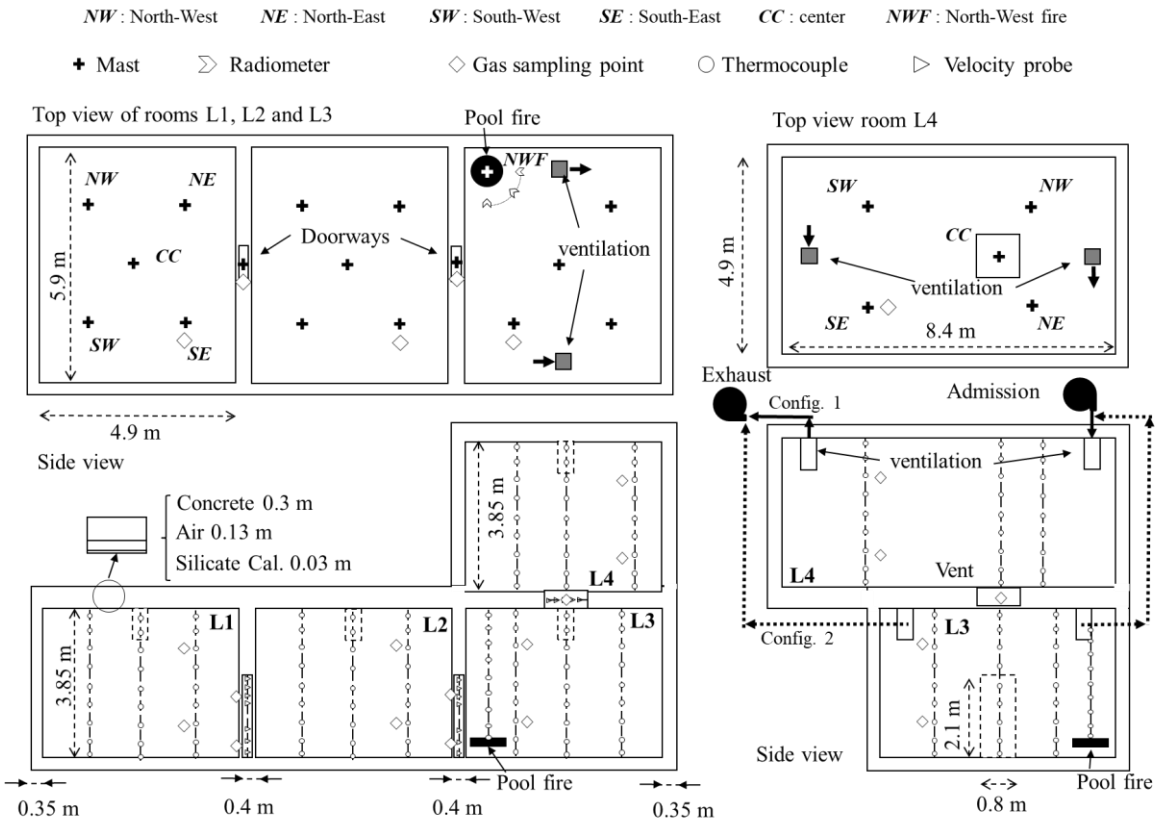

Fig. 2. Sketches of the facility

Fig. 3. Pictures of the installation: (a) fire room L3, (b) doorway between rooms L2 and L3 (c) view of the vent from room L4, (d) adjacent upper room L4

The measurement uncertainties were evaluated from calibration tests performed before and after the fire tests and from the characteristics of the sensors provided by the manufacturers. The calibration tests consisted in determining the difference between a reference measurement obtained by a standard source and the measurement read on the acquisition system. Two levels of uncertainty were adopted, following the procedure proposed by Hamins [28]. The standard uncertainties were obtained at room temperature without fire. A second level of uncertainty (expanded uncertainty) was defined through a coverage factor to take

into account the conditions during a fire test and the effects of repeatability (Table 1). The elaborated quantities were calculated from the raw data. The mass flow rates of gas at the doorway were calculated by integrating the vertical profiles of velocity and by taking into account the temperature profile and a discharge coefficient obtained from calibration tests [29] [10]. The flow rate at the vent was also calculated similarly from fourteen K-type thermocouples and bidirectional velocity probes distributed over the area [30]. The uncertainty on these global quantities was estimated at 20%, considering the uncertainties of all parameters included in the calculation process.

Table 1: Measurement uncertainties of raw quantities.

Physical variable	Range	Standard Uncertainty	Coverage Factor	Expanded Uncertainty
Mass	(0-300) kg	0.002 kg	2	0.004 kg
Gas temperature	(0-1300) °C	2°C	2	4°C
Plume temperature	(0-1300) °C	8°C	2	16°C
Gas velocity	(-2.3;+2.3) m/s at 20°C	5% (relative)	2	10% (relative)

2.3 CALIF^{3}S-Isis CFD tool

The two scenarios were numerically simulated with the CFD CALIF^{3}S-Isis software (free download from the following website: https://gforge.irsn.fr/gf/project/isis/). This tool developed by IRSN is a computational code based on low-Mach-number approximation originally dedicated to simulating fires in mechanically ventilated compartments. The balance equations [31], [17] were written for a low-compressibility flow, using a low-Mach-number approach. In this approach, the total pressure was split into three contributions: the thermodynamic, dynamic and hydrostatic pressures. The thermodynamic pressure is constant in space, the dynamic pressure depends on both time and space, and the hydrostatic part varies only with height z. The thermodynamic pressure is a function of time [32] and is expressed through the overall mass balance equation, considering the mass flow rate through all branches of the ventilation network connected to the compartment. In addition, a momentum balance equation based on a stationary Bernoulli equation was stated for each branch of the ventilation network.

To address the turbulent nature of the flows, a large-eddy simulation (LES) approach was used, in which the transport equations are solved for a filtered velocity field that describes the large-scale turbulent eddies. In this approach, a box filter in each direction is implicitly applied. The influence of the small-scale turbulent motions is represented by the WALE (Wall Adapting Local Eddy) subgrid-scale model for the subgrid Reynolds stress [33] in the simulations. Standard wall functions were used to consider the boundary layers near the walls where viscous effects are predominant. Turbulent combustion was based on the infinitely fast chemistry conserved scalar approach using the mixture fraction and the fuel mass fraction. The mean reaction rate, controlled by the turbulent flow mixing, was determined by the Eddy-Dissipation Combustion (EDC) model [34]. A one-step irreversible combustion reaction was considered for the fuel, which involves oxygen and products in the presence of a neutral gas. Among the different approaches available in CALIF^{3}S-Isis to model soot production and transport, the simplest approach with a coefficient (called soot conversion factor, ν_s) was considered in the single one-step reaction [35]. The radiative transfers were dealt with by the finite volume method [36] assuming a gray and non-scattering medium. The gas absorption coefficient of the mixture used the total emissivity approach of the weighted sum of gray gases model (WSGGM) and the soot absorption coefficient was related to the soot volume fraction according to the Mie theory. Wall conduction was taken into account through the 1D Fourier's equation, and the convective flux was given by standard laws based on laminar and turbulent Prandtl numbers [37]. The reader is referred to Appendix A of [31] for a detailed presentation of the governing balance equations solved by CALIF^{3}S-Isis software i.e. the Navier-Stokes equations, chemistry, enthalpy and radiative transfer. Finally,

concerning the boundary conditions, the experimental mass loss rate was imposed on the fire source area, and the classical boundary conditions were applied to the walls.

In the fire room, to correctly model the fire source, a refined Cartesian grid with a uniform square mesh ($\delta x \times \delta y$) was used over the subregion (denoted R1) covering the fire source. The horizontal grid spacing was kept constant in R1, namely $\delta x/r_o = \delta y/r_o = 0.1$ (with r_o the radius of the pool). In the horizontal x- and y-directions, to properly model the flow through the horizontal vent, a refined Cartesian grid with a uniform square mesh ($\delta x \times \delta y$) was also used over the subregion (denoted R2) that covers the horizontal vent. The horizontal grid spacing was kept constant in R2, namely $\delta x/r_o = \delta y/r_o = 0.1$, except close to the walls where the grid was shrunk. In the horizontal directions, between the subregions R1 and R2, the horizontal grid spacing was kept constant, namely $\delta x/r_o = \delta y/r_o = 0.15$. Finally, close to the walls and outside the subregions R1 and R2, the grid was shrunk toward the lateral boundaries of the computational domain. In the vertical z-direction, the grid spacing δz was uniform from the bottom boundary up to the vertical distance $Lz_1=H_d$, and then shrunk toward the upper boundary. The vertical grid spacing was kept constant over Lz_1, namely $\delta z/r_o = 0.15$. The choice of the grid spacings $\delta x/r_o$, $\delta y/r_o$ and $\delta z/r_o$ for the mesh checks for the satisfactory refinement criteria is referenced in the papers [38], [39], in which previous simulations compared successfully the LES approach on turbulent miscible Boussinesq and non-Boussinesq flows with experimental data and confirmed the suitability of the CALIF^{3}S-Isis code to properly evaluate the behaviours of turbulent buoyant flows exhibiting large density differences. The choice of the grid spacing was also guided by large-eddy simulations carried out for an elevated pool fire scenario in the same PRISME3 campaign, the results of which are in close agreement with the large-scale experiment [40].

Considering the mesh used in the adjacent rooms L2 and L1, in the horizontal x-direction, the grid spacing is kept constant, namely $\delta x/r_o = 0.25$ and is shrunk toward the lateral boundaries of the computational domain. In the horizontal y-direction, the grid spacing was kept constant $\delta y/r_o = 0.1$ over the width of the door (similar to the grid spacing over the subregion R2 in the fire room), kept constant, namely $\delta y/r_o = 0.35$, outside this region and shrunk toward the lateral boundaries of the computational domain. In the vertical direction, the grid spacing was kept constant, namely $\delta z/r_o = 0.15$ over the height of the door (similar to the vertical grid spacing used in the fireroom), kept constant, namely $\delta z/r_o = 0.4$, outside this region and shrunk toward the lateral boundaries of the computational domain. Finally, for the mesh used in upper room L4, in the horizontal directions, except the subregion R2 where the grid spacing was kept constant $\delta x/r_o = \delta y/r_o = 0.1$, the grid spacing was kept constant, namely $\delta x/r_o = \delta y/r_o = 0.35$ and shrunk toward the lateral boundaries of the computational domain. The vertical grid spacing was kept constant $\delta z/r_o = 0.15$ and shrunk close to the ceiling.

The reader interested in assessing the grid sensitivity of the computed solutions is referred to the work of Vaux et. al. [40] for similar LES simulations of large-scale fire experiments of the PRISME3 campaign in the same experimental facility DIVA. Two other meshes were tested in their study, by multiplying the grid spacing in each direction by a factor 1.2 and by 0.5, respectively. The grid convergence was assessed for gas temperature at two points on the south-west thermocouple tree. It is worth mentioning that no differences greater than 5 – 10 °C were observed in the hot upper layer (corresponding to a relative difference on the order of 1 − 2%). This is considered as satisfactory for simulations of real large-scale fire scenarios. We also refer the reader to papers [41], [42] for the sensitivity analysis and the validation of the CALIF^{3}S-Isis code.

3 Results

3.1 Fire source

The time variations of the fire mass loss rate (MLR) are shown in Fig. 4. The behaviour is first characterized by a progressive increase; this is followed by a steady period and then a smooth decrease toward extinction. The fire duration is longer for the 1 m^2 pool fire test because of a larger mass of fuel (17 kg for scenario A1 and 85 kg for scenario A2). The amplitudes of the MLR are lower than the levels in open atmosphere indicated in the figures from the Babrauskas correlation [43] using the input parameters

$k\beta$ = 1.32 m^{-1} and $\dot{m}_{\infty}$ = 35 g/s. Because of the oxygen vitiation around the fire area, the burning rate was reduced in comparison to the levels obtained in open atmosphere. The HRR was deduced from the MLR with consideration for the combustion enthalpy and a combustion efficiency of 1. The steady amplitude was about 200 kW for the 0.4 m^2 pool fire test and 600 kW for the 1 m^2 pool fire test. Regarding the numerical simulations, the fire HRR was not predicted; the experimental value obtained during the fire tests was set as the boundary condition.

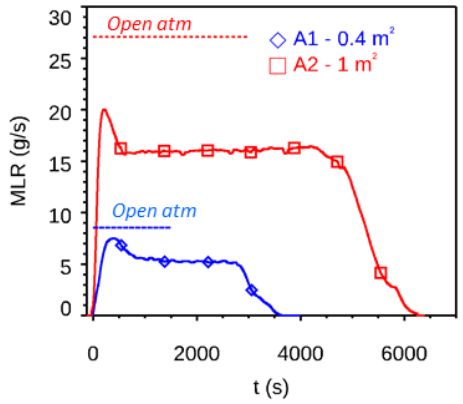

Fig. 4. Temporal evolution of the experimental MLR (the open atmosphere levels in dotted lines are derived from the Babrauskas correlation [43]).

3.2 Thermal stratification in the rooms

Thermal stratification is analysed on the basis of the temporal evolution of gas temperatures in the fire room. Fig. 5 shows the temporal evolution of temperatures obtained from the experiments (for 5 elevations z=0.05 m, z=1.05 m, z=2.05 m, z=3.05 m and z=3.85 m) and from the simulations (for two elevations at z=2.05 m and z=3.05m). The time trend shows a rapid increase after ignition followed by a slower gradual increase corresponding to the stationary phase of the MLR. The numerical simulations are in good agreement with the experimental data, illustrating the satisfactory prediction of the fire dynamics.

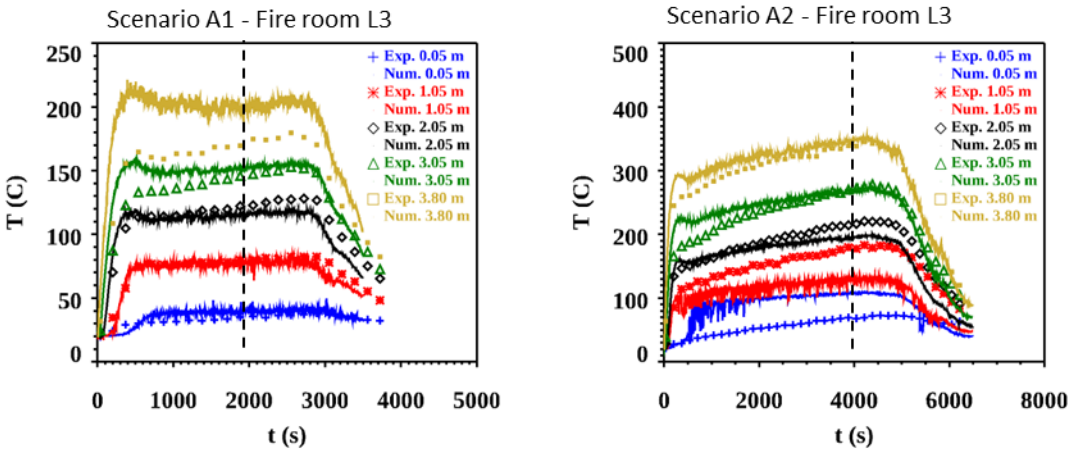

Fig. 5. Time variations of gas temperature on the NE axis in fire room L3 for the two scenarios A1 and A2 (data from fire tests are shown with symbols, data from simulations are shown with lines).

The vertical stratification in all rooms was analyzed on the basis of vertical temperature profiles at a given time during the steady period, 2000 s for scenario A1 and 4000 s for scenario A2 (Fig. 6). The vertical temperature profiles show progressive stratification with a constant gradient, typical of stratification in confined environments, as opposed to the homogeneous two-layer stratification found in ventilated enclosures with free intake. The temperature is maximum in the fire room (170 °C and 350° C for scenario A1 and A2 respectively) and decreases in the adjacent rooms, mainly because of the heat losses through walls and the mixing of smoke with air present in the rooms. In the two adjacent rooms (adjacent room L2 and upper room L4) connected to the fire room, the temperature is maximum in room L2 connected to the fire room by the doorway. Upper room L4 connected to the fire room with the vent undergoes a reduced temperature rise. This is mainly explained by the smoke release, which is much larger at the doorway than at the vent. Heat losses, larger in the upper adjacent room L4 because of a larger room area, may also explain the results. Comparison between the temperature of adjacent rooms L1 and L2 shows, as expected, a lower temperature in the farthest room (room L1). This is also explained by heat losses reducing the gas temperature and the mixing with non-vitiated air. It is important to note that the gas temperature in room L1 and room L4 are similar. This distribution of temperature within the rooms is very similar for the two scenarios. Only amplitudes are different with higher temperature for the 1 m^2 pool fire (scenario A2) because of a higher fire HRR. The maximum temperature is about 320° C in the fire room, 140 °C in adjacent room L2 and about 80°C in adjacent rooms L4 and L1. This similarity indicates that the geometry of the rooms and their arrangement (three rooms in a row and one above the fire room), which is identical for both scenarios, has a greater influence than the ventilation configuration.

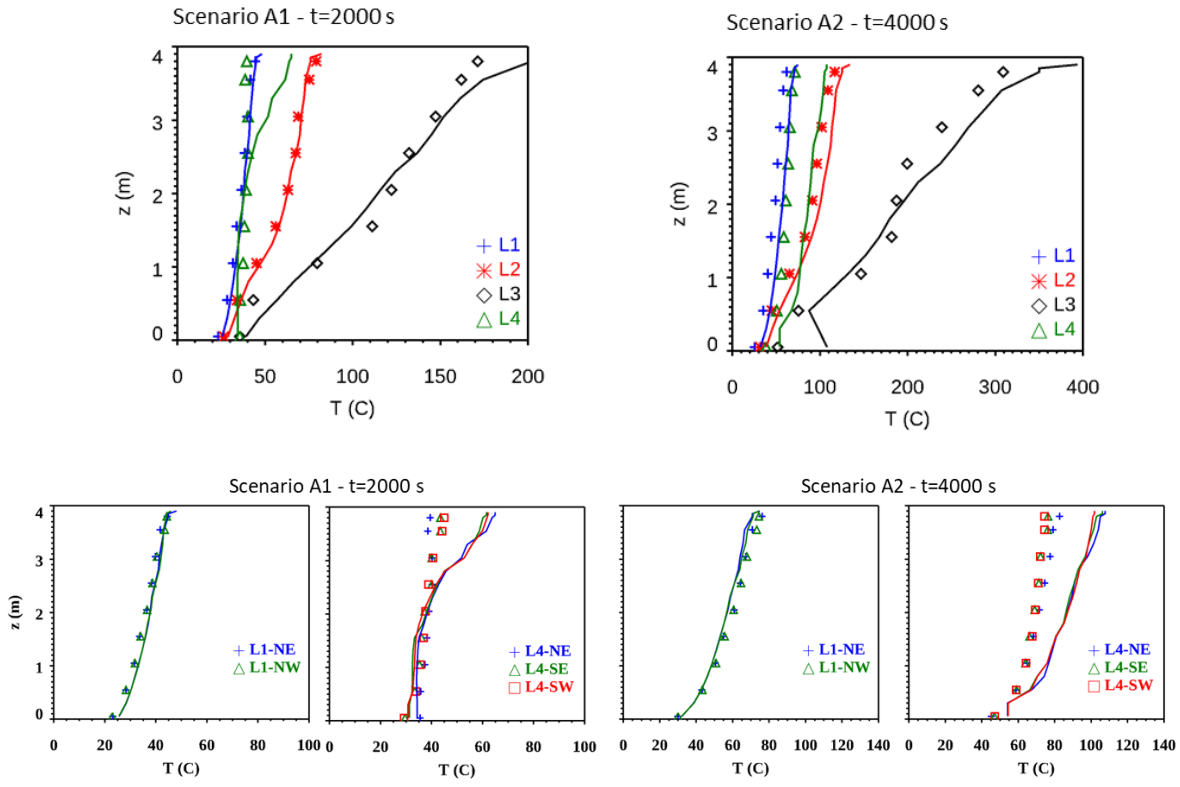

Fig. 6. Temperature profiles at a given time (2000 s for scenario A1 and 4000 s for scenario A2) in the four rooms L1, L2, L3 and L4 at the NE mast location (top) in the rooms L1 and L4 at three locations (bottom) (data from fire tests are shown with symbols, data from simulations are shown with lines).

The performance of the numerical simulations for predicting the thermal stratification was also analyzed for both scenarios. In room L3, the comparison is satisfactory in the upper part, but shows some slight differences in the lower part. This may be due to the interaction between the downward flow of fresh air through the horizontal vent and the flows in the lower part of L3 (in particular the fresh air flow from the lower part of the door). This interaction leads to highly three-dimensional, unsteady and complex flows in the lower part and the comparison between simulation and experiment is therefore easily affected in this area. In adjacent room L2, the profile is very well reproduced over the whole height of the room, with a deviation not exceeding 5 degrees. The gradients are also well reproduced, reflecting the good assessment of the thermal stratification. Within room L1, the thermal field is also well reproduced with temperatures varying by about 50 °C over the height of the compartment. Within room L4, the thermal field is more difficult to reproduce numerically due to a more complex 3D flow induced by the smoke release at the vent. This result illustrates the challenge of predicting the spread of smoke through a low-ventilation room.

In order to compare the shape of the vertical stratification between the two scenarios, dimensionless temperatures are obtained by scaling with the maximum temperature in the fire room $(T(z)-T_{ref})/(T_{max}^{L3}-T_{ref})$ with $T_{ref} = 20°C$, $T_{max}^{L3} = 154$ °C for scenario A1 and $T_{max}^{L3} = 302$ °C for scenario A2 (T_{max}^{L3} is the maximum temperature outside the flame in room L3). Results are presented in Fig. 7. Astonishingly, the dimensionless profiles are nearly self-similar. For the two scenarios with different fire HRRs, the maximum dimensionless temperature increase drops down to 0.4 in adjacent room L2 and to 0.18 in adjacent rooms L1 and L4. This result indicates that the process of temperature decay throughout smoke propagation towards connected rooms can be scaled with the fire HRR. Whatever the fire source amplitude, smoke propagation and temperature decrease are similar. The dimensionless temperature profiles also highlight differences of stratification in rooms L1 and L4. Although maximum temperatures below the ceiling are similar, the profile shapes are significantly different, with a flatter profile for the stratification in room L4. This difference is attributed to the way the smoke is released in the room, with a spill plume through a doorway in room L2 or with a vertical plume from the floor in room L4. In addition, the temperature profile in upper adjacent room L4 is the one that shows the largest difference between the two tests. This is attributed to the effect of the ventilation in this room, which is mechanical for the test with 0.4 m^2 pool fire and natural for the test with 1 m^2 pool fire.

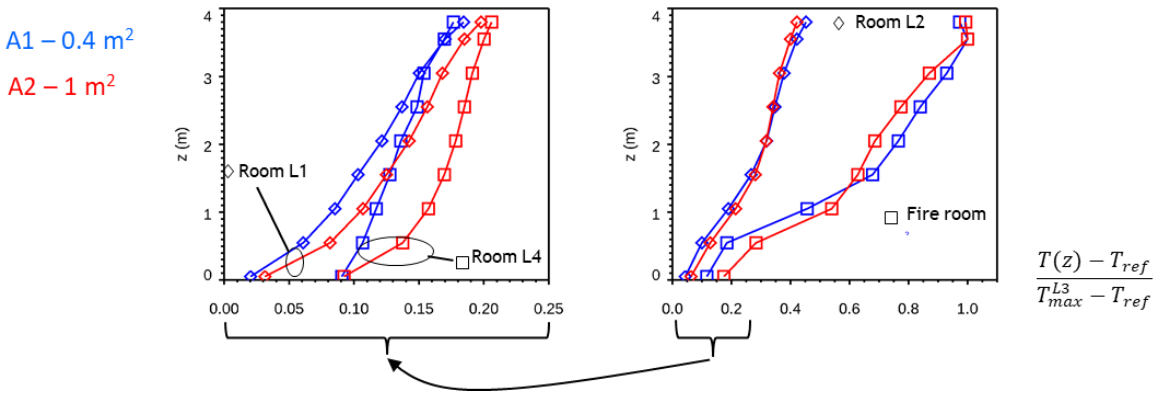

Fig. 7. Comparison of the dimensionless vertical temperature profiles at steady state in the four rooms for the two scenarios.

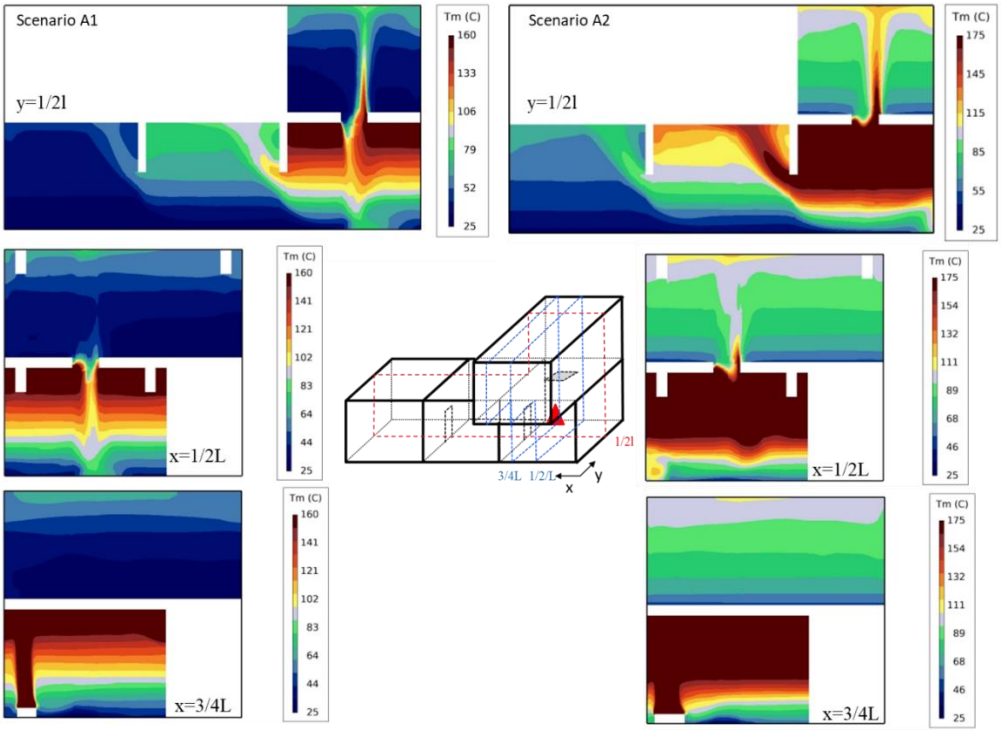

Fig. 8. Temperature field in several planes for the two scenarios

Despite the large number of experimental sensors for this type of large-scale experiment, it is unfortunately not possible to have a detailed map of the flows and thermal stratification in each room from the experiment alone. The experiment gives us well-defined zones (NE, NW, SE, SW masts, doorways and vents) for which CFD can be compared. Once this comparison has been validated, as is the case here, the CFD can provide a comprehensive range of flows for each scenario.

To illustrate the complementarity between simulations and experiment, the temperature fields in the rooms obtained from the numerical simulations can be used to visualize the thermal stratification identified from the experimental temperature profiles. The various planes shown in Fig. 8 allow us to identify the location of the fire in one of the corners of room L3, the fire plume, the two upward and downward plumes induced at the horizontal vent between room L3 and L4 and the spill plumes at the top of the two doorways. Apart from these local flows, which ensure mass transfer between rooms, thermal stratification is found in all the rooms. As can be seen from the profiles, temperatures are highest in the fire room for scenario A2, and lowest in room L1 for scenario A1.

3.3 Flows at the openings

3.3.1 Doorway flow

The experimental and numerical temperature and horizontal velocity profiles at the two vertical masts for the two doorways are presented in Fig. 9. Velocity profiles show a typical bidirectional shape with outflows of hot smoke in the upper part and inflow of cold fresh air in the lower part. The maximum velocity is greater for the smoke flow than for the fresh air because of the gas temperature. A maximum smoke velocity of about 2 m/s was obtained for scenario A2 with 1 m^2 pool fire. The amplitudes are, as expected, greater for the test with a larger pool size (1 m^2) associated with the highest HRR; they are also larger for

the doorway connected to the fire room. The results also show that the position of the neutral plane is around half of the total height. All these features are in agreement with the theory [1].

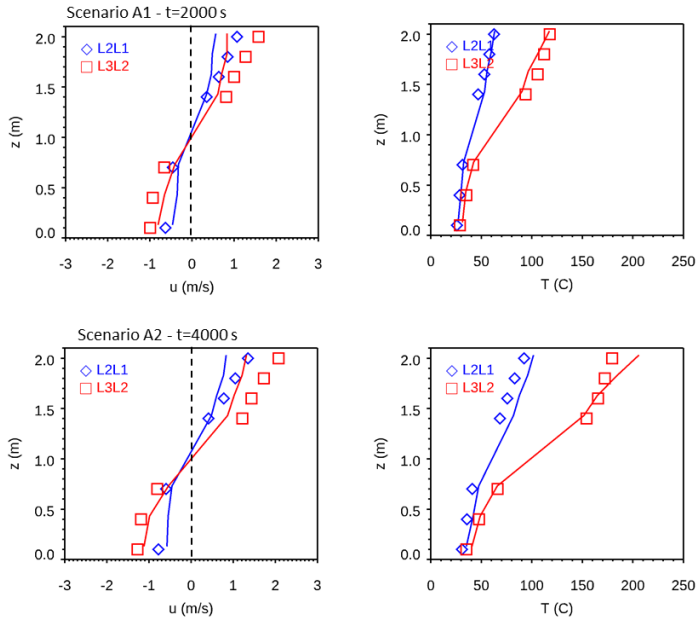

Fig. 9. Experimental (symbols) and numerical (lines) temperature and horizontal velocity profiles at the two vertical masts for doorways L2L1 and L3L2 during the steady stage (t = 2,000 s for scenario A1 and t = 4,000 s for scenario A2)

The measurements and numerical simulations give very similar results. General trends are reproduced satisfactorily, although there are some local differences in the evaluation of the velocity. On the other hand, a good estimate of the vertical temperature gradient is noted. Based on this satisfactory validation regarding velocities at the doorway, the horizontal velocity component can be analyzed in the doorway section and is presented in Fig. 10. The vertical thermal stratification reported in the rooms is also observed at the doorway with horizontal iso-temperature curves. Regarding the velocities, more variations are reported along the spanwise axis (i.e. the width of the doorway), especially for doorway L3L2 connected to the fire room. This behaviour is explained by the lateral flows induced in the fire room due to the position of the off-centre fire, the position of the vent and the mechanical ventilation for scenario A2. The results also show that the neutral plane is significantly higher for doorway L2L1 than for doorway L3L2, which is consistent with the fact that the velocity amplitude at the top of the doorway is higher for doorway L3L2.

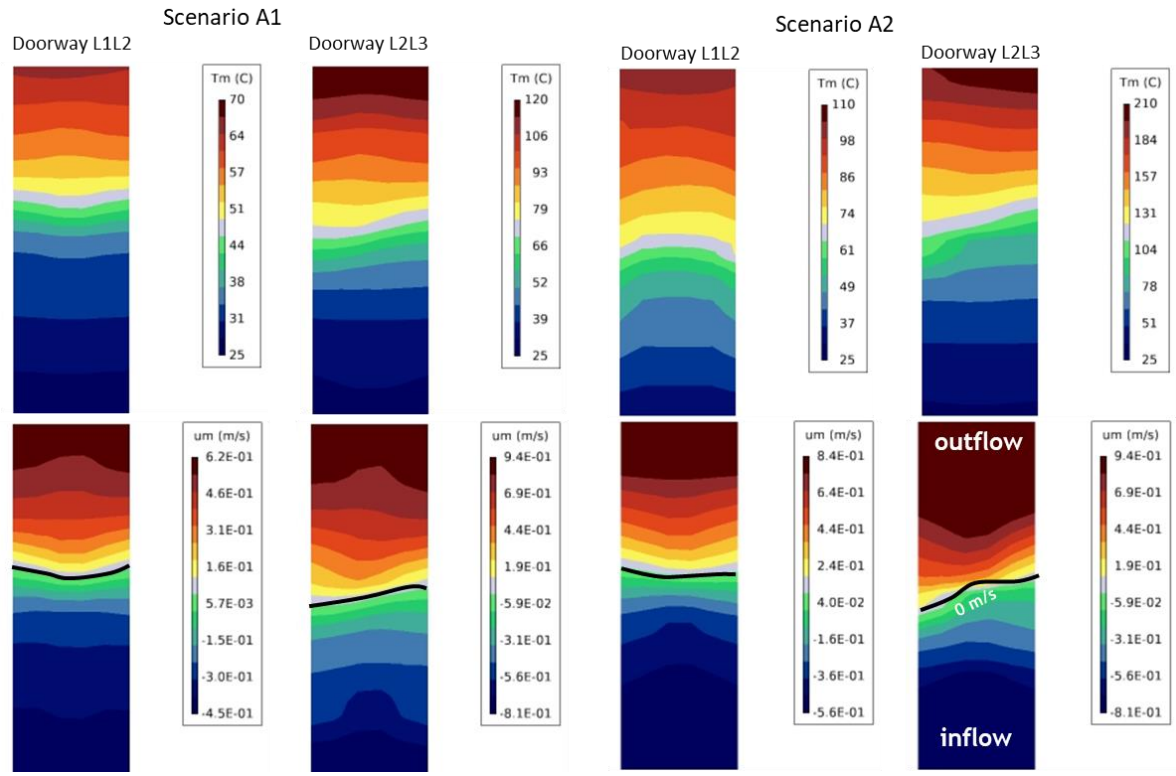

Fig. 10. Field of the u component of the velocity at the two doorways L2L1 and L3L2 during the steady stage (t = 2,000 s for scenario A1 and t = 4,000 s for scenario A2)

The analysis of the mass flow rate (in kg/s) through the openings, represented in figure 11, is performed considering the integration of the velocity field and the density field over the opening section. The amplitudes are nearly constant during the steady stage of the fire. For each doorway and for both scenarios, the inflows and outflows are of the same amplitude, which is a typical feature of flows at openings dominated mainly by natural convection and thus buoyancy (Fig. 11). If mechanical ventilation had had any effect, it would have unbalanced the two flows, one being higher than the other. Mechanical ventilation has little effect on these flows. For both scenarios, the mass flow rates are greater at doorway L3L2 than at doorway L2L1 due to the proximity of the fire, which induces higher temperatures and therefore higher buoyancy forces. This result corroborates the observations made for the higher velocity amplitudes at the L3L2 doorway. It is worth noting that the flow rates are greater for scenario A2 because of the greater fire HRR. The comparison between the experimental data and the numerical simulations shows similar behaviour. However, differences in amplitude are observed. The flow between fire room L3 and neighbouring room L2 shows a difference of about 20% between the experimental and simulated results. This discrepancy is explained by the limited number of test sensors (thermocouples and velocity probes) distributed over the height of the doorway, which prevents accurate calculation of the inflow and outflow. For such a calculation, numerical simulations are more appropriate.

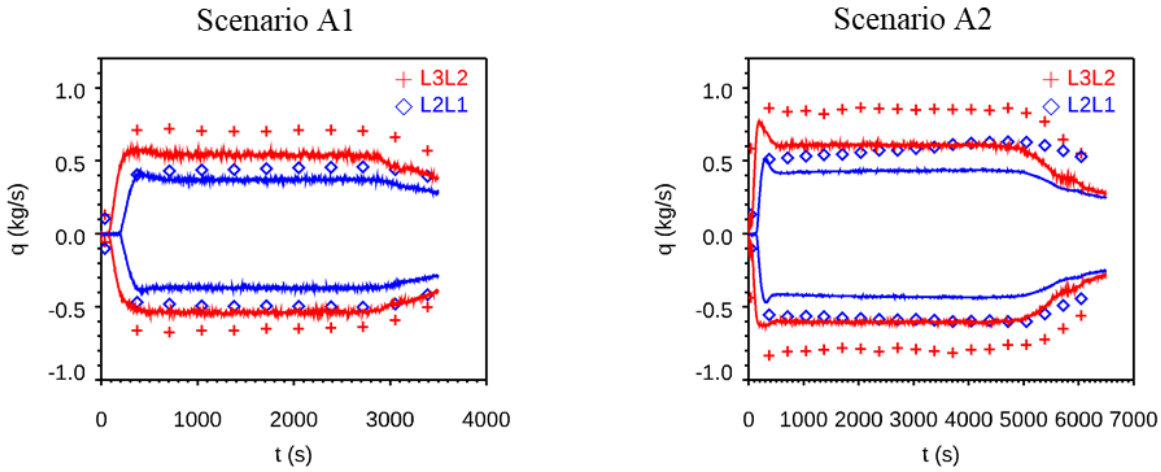

Fig. 11. Experimental (symbols) and numerical (lines) time variations of the outflow of smoke (positive) and inflow of fresh air (negative) at the two doorways and for the two scenarios.

3.3.2 Vent flows

The flow at the vent is first analysed from horizontal profiles of the vertical component of the velocity and temperature along two diagonals through the section (Fig. 12) as well as over the cross-section of the opening (Fig. 13). The flow also exhibits bidirectional behaviour, with an outflow of smoke (from the fire room to the upper room) and an inflow of fresh air (from the upper room to the fire room). However, unlike the doorway, the flow at the vent is more complex because of the horizontal cross-section, which does not allow a privileged zone to be created for the two flows. Recent works by Varrall.[44], [45] [46] have highlighted the fact that such flows do indeed exhibit pronounced instationarity. The profiles along the two diagonals and the velocity fields show that the upward flow of smoke is located on one side of the vent, leaving room for the downward flow on the remaining section. This behaviour is induced by the direction of flow of the ceiling jet, which is itself linked to the position of the fire in one corner of the room. This explanation is illustrated in more detail by the temperature field shown in Fig. 14. In this figure, the thermal field in two characteristic vertical planes of the fire room is represented. These planes pass through diagonals DIA1 and DIA2 of the horizontal vent. The results show a difference in the flows at the vent between the two scenarios, resulting in a shift in the sections carrying the upward and downward flows. This change is explained by the difference in fire HRR but also by the role of mechanical ventilation. The fields shown in Fig. 14 also show the flow of the descending cold plume, which constitutes the flow of fresh air feeding the fire. This flow crosses the smoke layer before diffusing into the lower part of the room. Figure 14 highlights the contribution of CFD to this type of complex flow in large-scale fires.

The results show generally good agreement between the numerical and experimental results in terms of general trends. The velocity and temperature amplitudes and the location of the flow cross-sections are, on the whole, well matched. The numerical simulations provide a more detailed description of the flows in the vent section than the measurement points. The intrusive measurement setup only allows general trends to be understood, but does not allow a detailed description such as that obtained numerically.

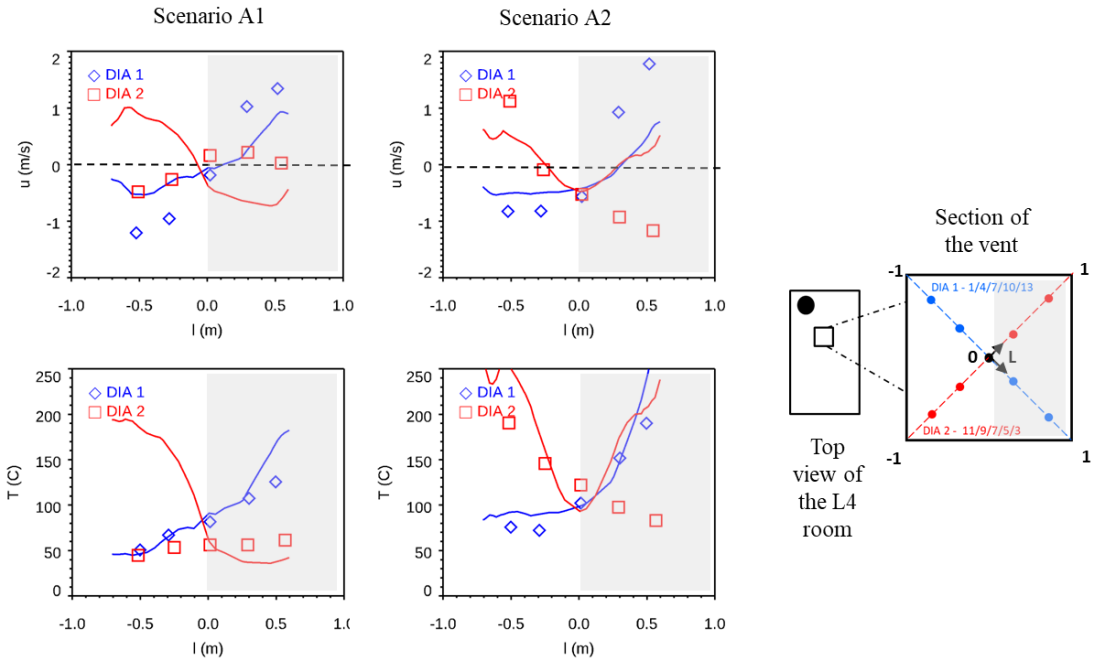

Fig. 12. Experimental (symbols) and numerical (line) temperature and velocity profiles along the two diagonals of the vent as illustrated on the sketch during the steady stage (t = 2,000 s for scenario A1 and t = 4,000 s for scenario A2)

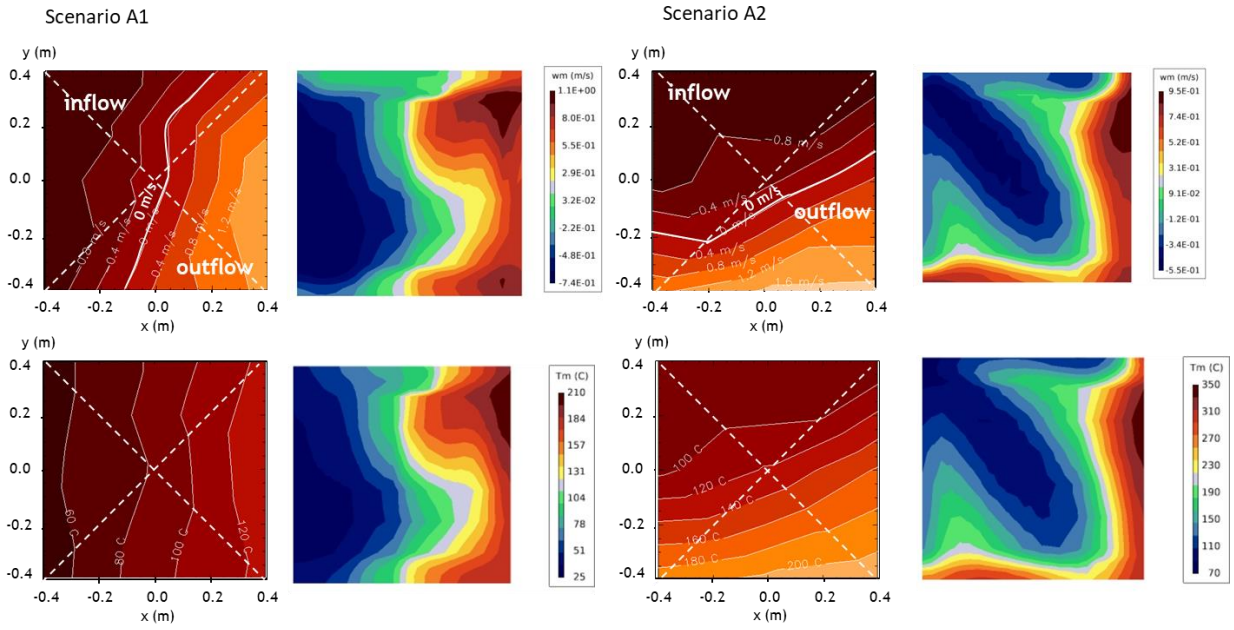

Fig. 13. Experimental and numerical temperature and velocity (w component) fields in the vent section during the steady stage (t = 2,000 s for scenario A1 and t = 4,000 s for scenario A2)

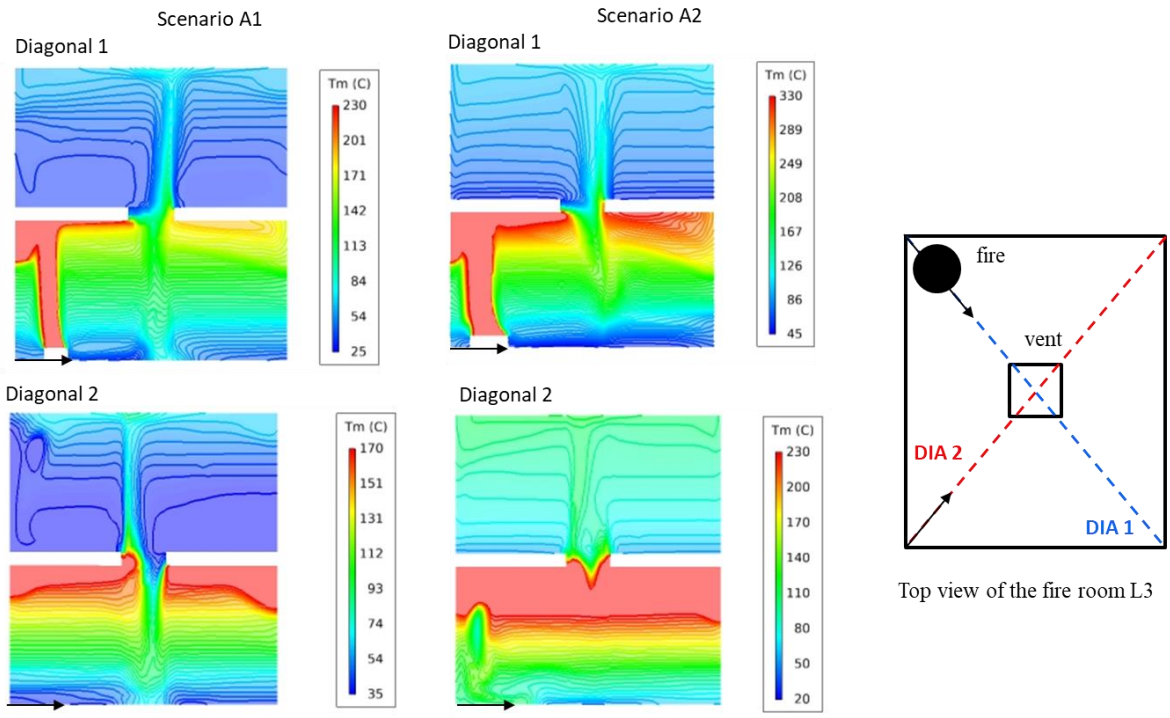

Top view of the fire room L3

Fig. 14. Numerical temperature fields in two planes (DIA1 and DIA2 as illustrated on the right sketch) in the fire room during the steady stage for the two tests.

On the basis of the velocity and temperature fields (numerical and experimental), the gas inflow and outflow rates are calculated by integration and presented in Fig. 15. Very good agreement is observed between the numerical and experimental data. As with the flows at the doorways, the upward and downward mass flow rates are of the same order of magnitude, indicating flows driven essentially by natural convection and buoyancy. The influence of mechanical ventilation on the amplitude of these flows is slight for these scenarios. In addition, the flows assessed (around 0.4 kg/s) are lower than those assessed at the doorways (~0.75 kg/s for L3L2 and ~0.55 kg/s for L2L1). The main reason for this is that the cross-sectional area of the vent is smaller than that of the doorway, leading to lower mass flow rate for similar temperature and velocity amplitudes.

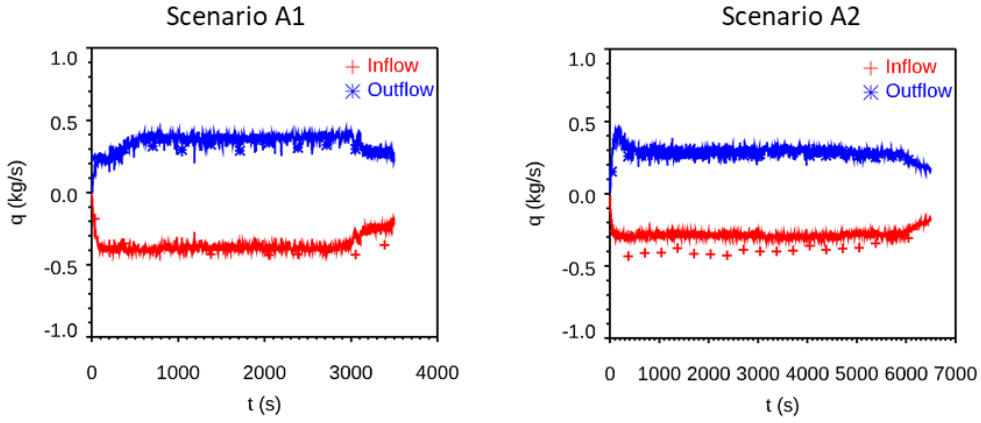

Fig. 15. Experimental (symbols) and numerical (line) time variations of the inflows and outflows at the vent for the two scenarios

3.3.3 *Discussion about the flow at the openings*

Good knowledge of the flow rates at the openings is essential to correctly assess smoke propagation and the supply of fresh air to the fire room. The different flow rates are determined from the spatial integration of the velocity and temperature over the opening area considered, at a time when the combustion regime is quasi-stationary (t = 2,000 s for test A1 and t = 4,000 s for test A2). Table 2 summarises the mass flow rates obtained numerically and experimentally for the three openings. For both scenarios, the flow rates at doorway L3L2 are the highest and those at the vent the lowest. The differences between measurements and simulations are on the order of 25%. The explanation for the discrepancies between experiments and simulations is a combination of measurement uncertainties, weaknesses in the modelling of turbulence, and heat transfer by radiation and heat losses. In the case of flow through an opening, the limited number of measurement points is a factor in reducing the accuracy of the integrated flow rate. Validation of the simulations with experimental data presented here is considered satisfactory for using the simulations in dead zone analysis. This discrepancy is, like other validation contributions, performed on large-scale fire tests. The FDS software was tested on a compartment fire in the work of Betting et al [47]. In this study, it was found that the thermal and velocity fields are correctly represented for well-ventilated cases, but that the software loses accuracy for under-ventilated cases. Furthermore, He et al [48] conducted a numerical and experimental study on fire-induced gas flow in a narrow ceiling compartment. Using FDS, their simulation fitted the experimental measurement to within 20%.

Table 2: Mass flow rates (in kg/s) at the three openings (the two doorways and the vent) at steady state, based on the experiments (Exp) and the numerical simulation (Sim).

			L1L2	L3L2	Vent
A1	Inflow (freshair)	Sim.	-0,37	-0,53	-0,38
		Exp.	-0,49	-0,66	-0,40
		Err(%)	28	20	3
	Outflow (smoke)	Sim.	0,37	0,54	0,37
		Exp.	0,45	0,70	0,31
		Err(%)	19	27	19
A2	Inflow (freshair)	Sim.	-0,43	-0,61	-0,30
		Exp.	-0,60	-0,80	-0,39
		Err(%)	31	27	26
	Outflow (smoke)	Sim.	0,44	0,61	0,30
		Exp.	0,62	0,85	0,28
		Err(%)	35	33	7

Given the acceptable agreement between the numerical simulations and the experimental data, the analysis of the total volume flows was carried out on the basis of the numerical simulations, which are considered to be more accurate than the experimental data. The distribution of volume flow rates into and out of each room is shown in Table 3 and illustrated in Fig. 16. The results show that the volume flow rates through the vent are significant and make a major contribution to smoke evacuation, but also to the supply of fresh air to the fire room. For both scenarios, it represents at least 40% of the total flow entering the fire room. This is an important result and underlines the need for appropriate modelling of vent flows in fire risk analyses. In such safety analyses, one of the crucial aims is to correctly predict the flow of outgoing smoke as well as that of incoming fresh gas and its diffusion towards the fire zone.

The results also indicate the amplitude of the total airflow into and out of each room, making it possible to quantify the air change rate per hour (ACH) or the renewal rate (Tr) for each room. This is calculated as the ratio between the total volume flow leaving the enclosure and the volume of the enclosure. The first result concerns the amplitude of the renewal rate for rooms that are only naturally ventilated, which is greater

than 11 h^{-1} and can reach 38 h^{-1}. These levels, which are much higher than the values commonly used for mechanical ventilation, show that the flows induced by buoyancy are equal to or greater than those induced by mechanical ventilation. During a fire, natural ventilation induced by the fire is the dominant mechanism governing the flows. For example, for scenario A1, the renewal rate of room L4 by mechanical ventilation is 14 h^{-1} before the fire and increases to 24 h^{-1} during the fire because of the additional flows induced by buoyancy. For scenario A2, the renewal rate of room L3 is 22 h^{-1} before the fire and increases to 50 h^{-1} during the fire. The results also show that the least ventilated rooms are those far from the fire and/or without mechanical ventilation. These are room L1 for scenario A1 and rooms L1 and L4 for scenario A2, which have a renewal rate below 15 h^{-1}. In view of these results, it is vital to have a well-qualified calculation code with fine models that can satisfactorily model the complex natural ventilation flows induced by fire.

Table 3: Numerical volumetric flow rates entering (in) and leaving (out) each room and the resulting renewal rate of each room considering the volume of each room (111 m^3 for room L1, L2 and L3 and 157 m^3 for L4) - Tr_o is the renewal rate before ignition.

		L1	L2	L3 (fire room)	L4
A1	In (m^3/h)	1160	2963	3810	3608
	Out (m^3/h)	1265	3223	2906	4147
	Tr (h^{-1})	11,4	29,0	26,2	26,4
	Tr_o (h^{-1})	-	-	-	15,29
A2	In (m^3/h)	1426	3684	6881	1107
	Out (m^3/h)	1640	4202	5552	1704
	Tr (h^{-1})	14,8	37,9	50,0	10,9
	Tr_o (h^{-1})	-	-	21,6	-

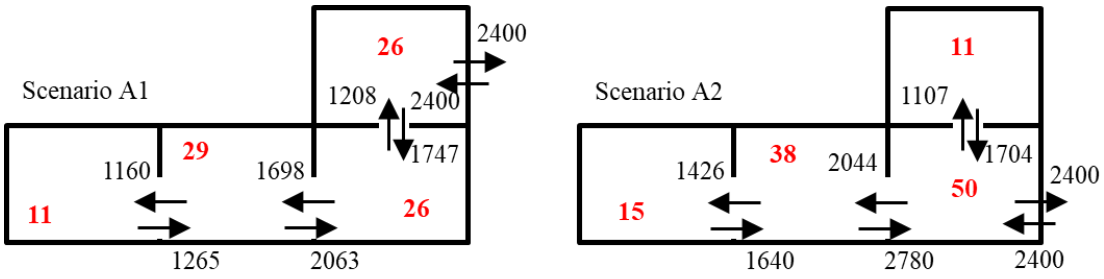

Fig. 16. Illustration of the numerical volume flow rate (in black and in m^3/h) entering and leaving each room and the renewal rate (in red and in h^{-1}) of each room during the steady stage based on the data given in Table 3

3.4 Flows in the non-mechanically ventilated rooms (dead zones)

An innovative aspect of this study is to address smoke flows in rooms that are not mechanically ventilated and in which the flows are driven solely by buoyancy. This concerns the least-ventilated rooms identified in the previous section: room L1 for scenario A1 and room L4 for scenario A2. In room L1 for scenario A1, Fig. 17 shows velocity fields in the XZ and YZ cross-sectional planes. The significant flow is that of the spill plume coming from the upper part of the doorway, which then propagates under the ceiling in a radial ceiling jet over a small thickness of approximately 0.5 m. The rest of the room has very low velocities of less than 0.075 m/s. The flow in this room results in smoke-filling in an almost stationary environment at rest. Similar velocity fields are shown in room L4 for scenario A2 in Fig. 18. In this room,

the rising plume from the vent is the dominant flow. It discharges vertically and then impacts the ceiling, resulting in a radial flow. The rest of the room has very low velocities, which in some areas are less than 0.075 m/s. These results for the two scenarios show that rooms that are far from the fire room and not mechanically ventilated are, like dead zones, naturally ventilated by a bidirectional flow supplying smoke and extracting less vitiated air. A large part of the volume of these rooms has velocities of less than 0.075 m/s.

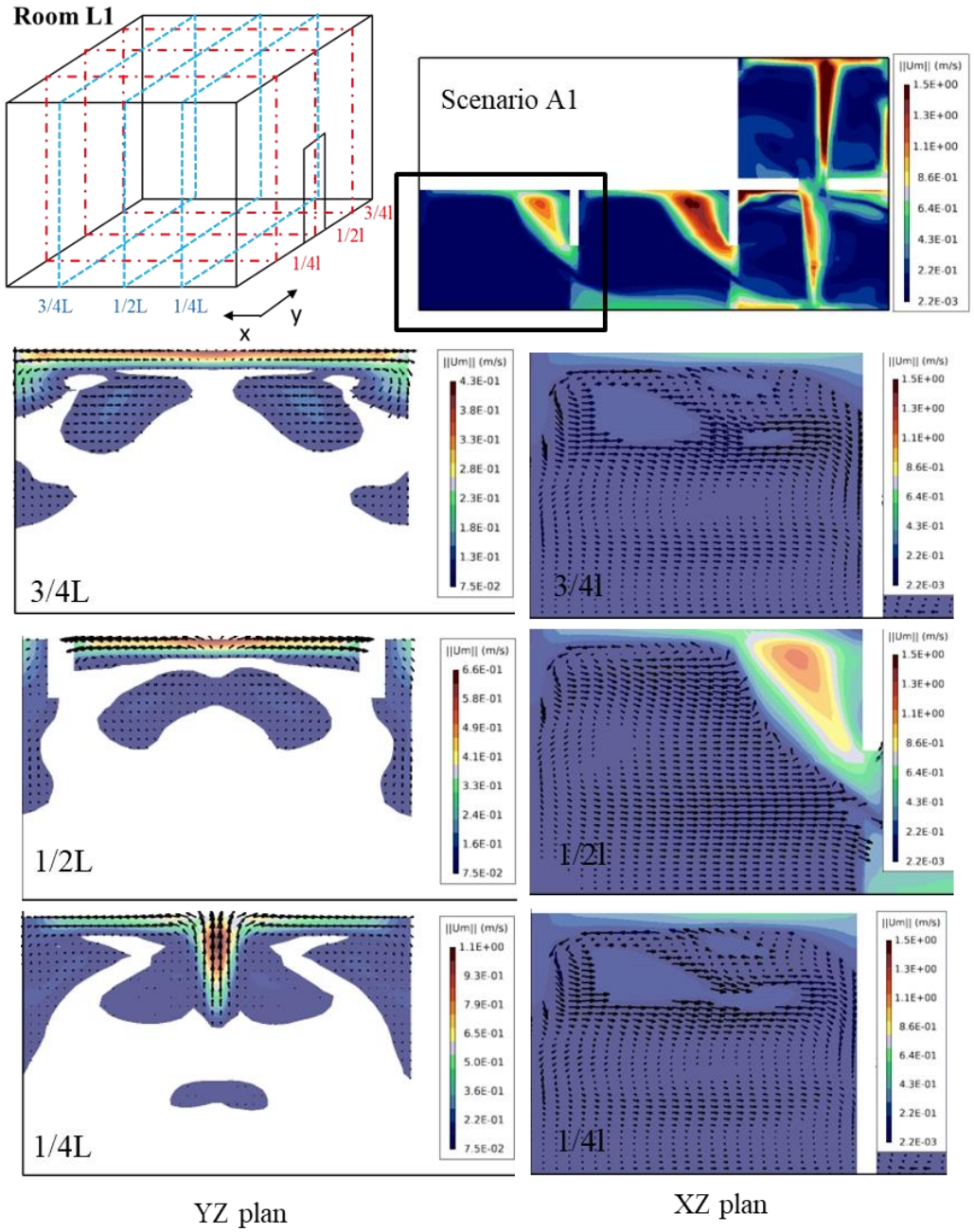

Fig. 17. Norm of the velocity and velocity vectors for the scenario A1 - XZ planes (only amplitude above 0.075 m/s is displayed), XZ planes (only vector amplitude below 0.075 m/s is displayed)

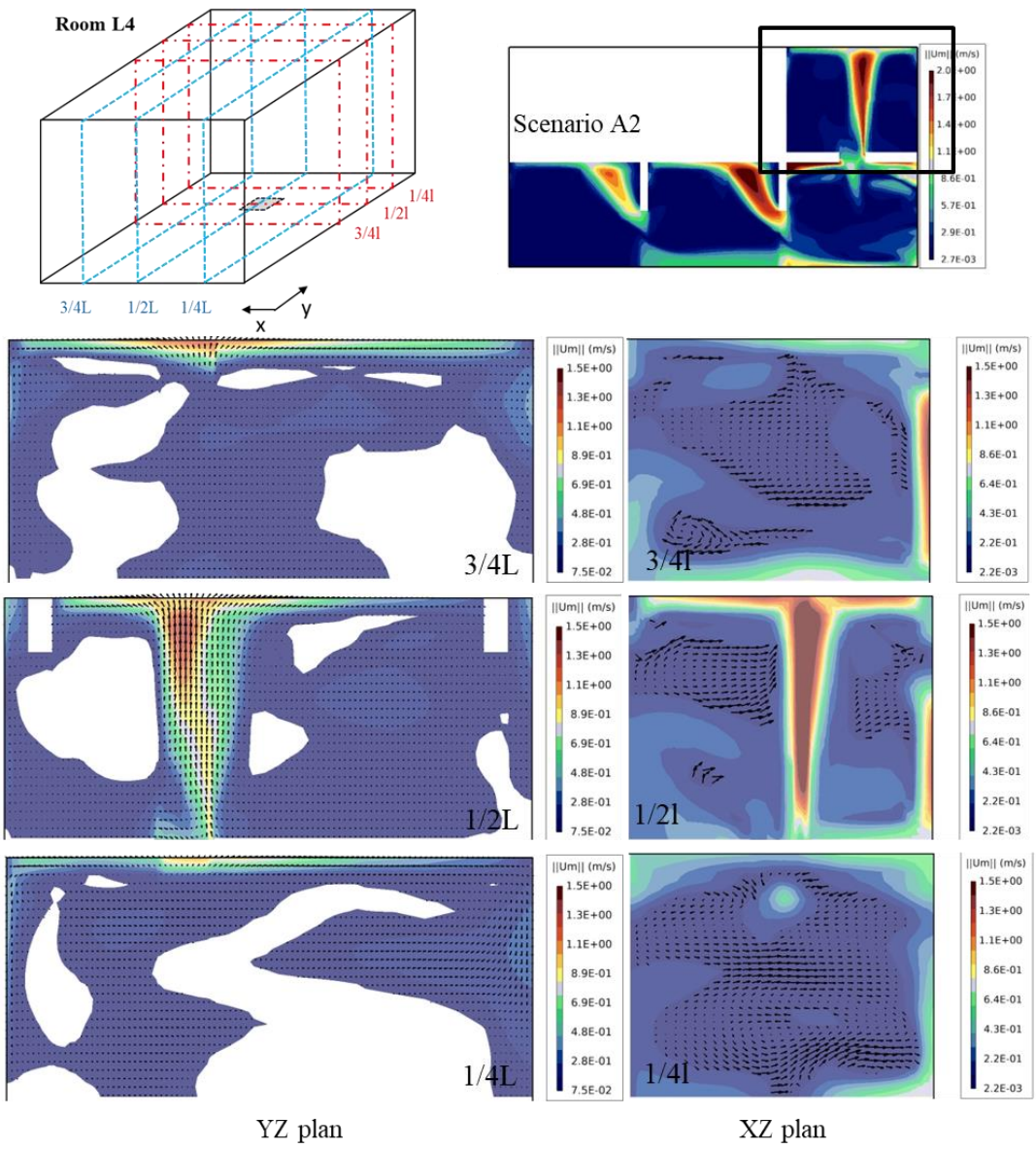

Fig. 18. Norms of the velocity and velocity vectors for the scenario A2 : XZ planes (only amplitude above 0.075 m/s is displayed), XZ planes (only vector amplitude below 0.075 m/s is displayed)

4 Conclusions

The study proposes an analysis of the fire-induced flows in a multi-compartment assembly in case of a fire event. The combination of two modes of propagation through doorways and vent, together with the effect of the fire source and of mechanical ventilation are investigated. The study is based on the analysis of two scenarios reproduced experimentally at large scale and numerically from simulations with a CFD code. The scenarios comprise a lubricant oil pool fire of about 200 kW and 600 kW in an assembly of four rooms connected with two doorways and a vent and mechanically ventilated with two different configurations representative of practical situations encountered in nuclear installations. The main outcomes are as follows:

- Smoke flows through the rooms induced vertical thermal stratification, with a constant gradient typical of stratification in confined spaces. Gas temperature decreased, with smoke propagating through the connecting rooms mainly because of heat losses through the walls and mixing with fresh air. The shape of the vertical temperature profile was found to be nearly self-similar, irrespective of the fire HRR.
- Flow through the doorway was the major transfer mode, although flow through the vent made a significant contribution (about 40%). Flow through the vent was bidirectional like that through the doorway but had a more complex structure. The downward part of this flow can be a major issue when it feeds the fire with oxygen.
- On the basis of numerical simulations, velocity fields in the rooms far from the fire room and not mechanically ventilated were investigated. A large part of the volume of these rooms corresponds to dead zones in which velocity amplitudes are below 0.075 m/s.
- The combined study of large-scale fire tests and numerical simulations shows good agreement between the two approaches concerning thermal stratification and flows at the openings. The results demonstrated the validity of CFD approaches for the evaluation of smoke flows in a configuration of several rooms connected to each other by doorways and vent. The results also show that the modelling of fire-induced natural ventilation flows is vital even for scenarios involving mechanically ventilated enclosures.

The outcomes of this study provide a new understanding of fire-induced flows in an assembly involving four confined and ventilated compartments. They also demonstrate the ability of the CFD approach to deal with complex configurations in fire risk assessment and to provide additional information not accessible through experiment.

5 Acknowledgements

The authors would like to thank all the partners involved in the OECD/NEA PRISME 3 project for their financial support and the fruitful discussions throughout the project.

6 References

[1] K. D. Steckler, J. G. Quintiere, and W. Rinkinen, “Flow induced by fire in a compartment,” *Int. Symp. Combust.*, pp. 913–920, 1982.

[2] L. Y. Cooper, M. Harkleroad, J. G. Quintiere, and W. Rinkinen, “An experimental study of upper hot layer stratification in full scale multiroom fire scenarios,” *J. Heat Transfer*, vol. 104, p. 741, 1982.

[3] G. Heskestad, “Modeling of enclosure fires,” *Symp. Combust.*, vol. 14, no. 1, pp. 1021–1030, Jan. 1973, doi: 10.1016/S0082-0784(73)80092-X.

[4] G. Heskestad and T. Hamada, “Ceiling jets of strong fire plumes,” *Fire Saf. J.*, vol. 21, no. 1, pp. 69–82, 1993, doi: 10.1016/0379-7112(93)90005-B.

[5] P. H. Thomas, “Two-dimensional smoke flows from fires in compartments: some engineering relationships,” *Fire Saf. J.*, vol. 18, no. 2, pp. 125–137, 1992, doi: 10.1016/0379-7112(92)90035-B.

[6] J. Prahl and H. W. Emmons, “Fire induced flow through an opening,” *Combust. Flame*, vol. 25, no. C, pp. 369–385, 1975, doi: 10.1016/0010-2180(75)90109-1.

[7] R. D. Peacock, W. W. Jones, and R. W. Bukowski, “Verification of a model of fire and smoke transport,” *Fire Saf. J.*, vol. 21, no. 2, pp. 89–129, 1993, doi: 10.1016/0379-7112(93)90038-R.

[8] F. W. Mowrer, “Enclosure smoke filling revisited,” *Fire Saf. J.*, vol. 33, no. 2, pp. 93–114, 1999, doi: 10.1016/S0379-7112(99)00023-5.

[9] M. J. Peatross and G. L. Beyler, “Ventilation effects on compartment fire characterization,” in *Fire Safety Science, Proceeding of the Fifth International Symposium*, 1997, pp. 403–414.

[10] H. Prétrel, A. Koched, and L. Audouin, “Doorway Flows Induced by the Combined Effects of Natural and Forced Ventilation in Case of Multi-compartments Large-Scale Fire Experiments,” *Fire Technol.*, vol. 52, no. 2, pp. 489–514, 2016, doi: 10.1007/s10694-015-0524-8.

[11] H. Prétrel and J. M. Such, “Effect of ventilation procedures on the behaviour of a fire compartment scenario,” *Nucl. Eng. Des.*, vol. 235, no. 20, pp. 2155–2169, 2005, doi: 10.1016/j.nucengdes.2005.03.003.

[12] V. Novozhilov, “Computational fluid dynamics modeling of compartment fires,” *Prog. Energy Combust. Sci.*, vol. 27, pp. 611–666, 2001.

[13] F. Bonte, N. Noterman, and B. Merci, “Computer simulations to study interaction between burning rates and pressure variations in confined enclosure fires,” *Fire Safety Journal*. 2013. doi: 10.1016/j.firesaf.2013.01.030.

[14] L. Gay, B. Sapa, and F. Nmira, “MAGIC and Code-Saturne developments and simulations for mechanically ventilated compartment fires,” *Fire Saf. J.*, vol. 62, no. PART B, pp. 161–173, 2013, doi: 10.1016/j.firesaf.2013.01.017.

[15] S. Vaux and H. Prétrel, “Relative effects of inertia and buoyancy on smoke propagation in confined and forced ventilated enclosure fire scenarios,” *Fire Saf. J.*, vol. 62, no. PART B, pp. 206–220, 2013, doi: 10.1016/j.firesaf.2013.01.013.

[16] S. Suard, S. Hostikka, and J. Baccou, “Sensitivity analysis of fire models using a fractional factorial design,” *Fire Saf. J.*, vol. 62, no. PART B, pp. 115–124, 2013, doi: 10.1016/j.firesaf.2013.01.031.

[17] S. Suard, M. Forestier, and S. Vaux, “Toward predictive simulations of pool fires in mechanically ventilated compartments,” *Fire Saf. J.*, vol. 61, pp. 54–64, 2013, doi: 10.1016/j.firesaf.2013.08.010.

[18] A. Nasr, S. Suard, H. El-Rabii, L. Gay, and J. P. Garo, “Fuel mass-loss rate determination in a confined and mechanically ventilated compartment fire using a global approach,” *Combust. Sci. Technol.*, vol. 183, no. 12, pp. 1342–1359, 2011, doi: 10.1080/00102202.2011.596174.

[19] S. Vaux, H. Prétrel, and L. Audouin, “Experimental and numerical study of water spray system for a fire event in a confined and mechanically ventilated compartment,” *Fire Mater.*, no. February, pp. 579–590, 2019, doi: 10.1002/fam.2719.

[20] H. Prétrel and S. Vaux, “Experimental and numerical analysis of fire scenarios involving two mechanically ventilated compartments connected together with a horizontal vent,” *Fire Mater.*, vol. 43, no. 5, pp. 514–529, 2019, doi: 10.1002/fam.2695.

[21] J. Wahlqvist and P. van Hees, “Implementation and validation of an environmental feedback pool fire model based on oxygen depletion and radiative feedback in FDS,” *Fire Saf. J.*, vol. 85, pp. 35–49, 2016, doi: 10.1016/j.firesaf.2016.08.003.

[22] J. Wahlqvist and P. Van Hees, “Validation of FDS for large-scale well-confined mechanically ventilated fire scenarios with emphasis on predicting ventilation system behavior,” *Fire Saf. J.*, 2013, doi: 10.1016/j.firesaf.2013.07.007.

[23] O. Ukairo, S. Dembele, A. Heidari, H. Prétrel, and J. Wen, “Investigation of fires in a mechanically ventilated compartment using the CFD code FireFOAM,” *Nucl. Eng. Des.*, vol. 384, no. September, p. 111515, 2021, doi: 10.1016/j.nucengdes.2021.111515.

[24] D. Le, J. Labahn, T. Beji, C. B. Devaud, E. J. Weckman, and A. Bounagui, “Assessment of the capabilities of FireFOAM to model large-scale fires in a well-confined and mechanically ventilated multi-compartment structure,” *J. Fire Sci.*, vol. 36, no. 1, pp. 3–29, 2018, doi: 10.1177/0734904117733427.

[25] H. Prétrel and P. Querre, “Repeatability assessment of large-scale fire experiment involving water spray system in a forced ventilated compartment,” *Fire Mater.*, vol. 43, no. 5, pp. 436–447, 2019, doi: 10.1002/fam.2679.

[26] K. Tasaka, K. Shirai, J. Ji, and P. Zavaleta, “Experimental study of smoke effects on energized electrical cabinets located nearby a lubricant oil pool fire,” *Fire Mater.*, vol. 43, no. 5, pp. 561–578, 2019, doi: 10.1002/fam.2718.

[27] S. Suard, P. Van Hees, M. Roewekamp, S. Tsuchino, and R. Gonzalez, “Fire development in multi-compartment facilities: PRISME 2 project,” vol. 43, no. September, pp. 433–436, 2019.

[28] A. Hamins and K. Mc Grattan, “Verification and Validation of Selected Fire Models for Nuclear Power Plant Applications Vol 2 - Experimental Uncertainty,” *Nureg-1824 -EPRI 1011999 Final Rep.*, 2014, [Online]. Available: http://scholar.google.com/scholar?hl=en&btnG=Search&q=intitle:Verification+and+Validation+of+Selected+Fire+Models+for+Nuclear+Power+Plant+Applications#0

[29] A. Koched, H. Prétrel, O. Vauquelin, and L. Audouin, “Experimental determination of the discharge flow coefficient at a doorway for fire induced flow in natural and mixed convection,” *Fire Mater.*, vol. 40, no. 1, pp. 114–128, 2016, doi: 10.1002/fam.2272.

[30] H. Prétrel, R. Sayada, K. Varrall, L. Audouin, and O. Vauquelin, “Experimental study based on large-scale smoke propagation fire tests through a horizontal opening connecting two mechanically ventilated compartments,” *Fire Saf. J.*, vol. 90, 2017, doi: 10.1016/j.firesaf.2017.02.007.

[31] “ISIS 6.0.0.: Physical Modelling, Institut de Radioprotection et de Surete Nucleaire, https://gforge.irsn.fr/gf/project/isis/.”.

[32] S. Suard, C. Lapuerta, F. Babik, and L. Rigollet, “Verification and validation of a CFD model for simulations of large-scale compartment fires,” *Nucl. Eng. Des.*, vol. 241, no. 9, pp. 3645–3657, 2011, doi: 10.1016/j.nucengdes.2011.08.012.

[33] F. Nicoud and F. Ducros, “Subgrid-scale stress modelling based on the square of the velocity,” *Flow, Turbul. Combust.*, vol. 62, pp. 183–200, 1999.

[34] B. F. Magnussen and B. H. Hjertager, “On mathematical modeling of turbulent combustion with special emphasis on soot formation and combustion,” *Symp. Combust.*, vol. 16, no. 1, pp. 719–729, 1977, doi: 10.1016/S0082-0784(77)80366-4.

[35] V. Novozhilov and H. Koseki, “CFD prediction of pool fire burning rates and flame feedback,” *Combust. Sci. Technol.*, vol. 176, pp. 1283–1307, 2004.

[36] J. Chai, H. Lee, and S. Patankar, “J. Chai, H. Lee, S. Patankar, Finite volume method for radiation heat transfer, J. of Thermophysics and Heat Transfer 8 (1994) 419–425.,” *J. Thermophys. heat Transf.*, vol. 8, pp. 419–425, 1994.

[37] G. Cox, *Combustion fundamentals of fire, Academic Press, 1995*. 1995.

[38] R. Mehaddi, S. Vaux, F. Candelier, and O. Vauquelin, “On the modelling of steady turbulent fountains,” *Environ. Fluid Mech.*, vol. 15, no. 6, pp. 1115–1134, 2015, doi: 10.1007/s10652-015-

9400-9.

[39] S. Vaux, R. Mehaddi, O. Vauquelin, and F. Candelier, “Upward versus downward non-Boussinesq turbulent fountains,” *J. Fluid Mech.*, vol. 867, pp. 272–291, 2019.

[40] S. Vaux, E. Georges, and H. Pretrel, “Experimental and numerical study of an elevated pool fire scenario in a confined and mechanically ventilated,” *Fire Saf. J.*.

[41] S. Suard, C. Lapuerta, A. Kaiss, and B. Porterie, “Sensitivity analysis of a fire field model in the case of a large-scale compartment fire scenario,” *Numer. Heat Transf. Part A Appl.*, vol. 63, no. 12, pp. 879–905, 2013, doi: 10.1080/10407782.2012.725010.

[42] S. Suard, A. Koched, H. Prétrel, and L. Audouin, “Numerical simulations of fire-induced doorway flows in a small scale enclosure,” *Int. J. Heat Mass Transf.*, vol. 81, pp. 578–590, 2015, doi: 10.1016/j.ijheatmasstransfer.2014.10.069.

[43] V. Babrauskas and S. J. Grayson, *Heat release in fires*. Interscience communications, 1990.

[44] K. Varrall, H. Prétrel, S. Vaux, and O. Vauquelin, “Improvement of Correlative Approaches for Mixed Convective Flow Through a Horizontal Vent,” *J. Heat Transfer*, vol. 141, no. 3, 2019, doi: 10.1115/1.4042330.

[45] K. Varrall, H. Prétrel, S. Vaux, and O. Vauquelin, “Stereoscopic particle image velocimetry investigations of the mixed convection exchange flow through a horizontal vent,” *Exp. Fluids*, vol. 58, no. 10, pp. 1–10, 2017, doi: 10.1007/s00348-017-2434-7.

[46] K. Varrall, H. Prétrel, S. Vaux, and O. Vauquelin, “Stereoscopic Particle Image Velocimetry Investigation of the Bidirectional Natural Convection Flow Through a Horizontal Vent,” *Fire Technol.*, vol. 52, no. 6, pp. 2027–2041, 2016, doi: 10.1007/s10694-016-0593-3.

[47] B. Betting, E. Varea, C. Gobin, G. Godard, B. Lecordier, and B. Patte-Rouland, “Experimental and numerical studies of smoke dynamics in a compartment fire,” *Fire Saf. J.*, vol. 108, no. May, p. 102855, 2019, doi: 10.1016/j.firesaf.2019.102855.

[48] Q. Z. He, J. T. Yang, and Y. F. Zhang, “Numerical simulation of fire induced gas flow in a narrow ceiling vented compartment,” *Procedia Eng.*, vol. 211, pp. 226–234, 2018, doi: 10.1016/j.proeng.2017.12.008.